IOP Publishing Journal of Physics: Condensed Matter
J. Phys.: Condens. Matter **32** (2020) 265401 (10pp) https://doi.org/10.1088/1361-648X/ab79f9

Evolution of two-step magnetic transition on nanogranular $Gd_5Si_{1.3}Ge_{2.7}$ thin film

J H Belo[1], A L Pires[1], I T Gomes[1], J B Sousa[1], R L Hadimani[2], D C Jiles[3,4], A M Pereira[1] and J P Araújo[1]

[1] IFIMUP, Departamento de Física e Astronomia da Faculdade de Ciências da Universidade do Porto, Rua do Campo Alegre, 687, 4169-007 Porto, Portugal
[2] Department of Mechanical and Nuclear Engineering, Virginia Commonwealth University, Richmond, Virginia 2328, United States of America
[3] Department of Electrical and Computer Engineering, Iowa State University, Ames, IA 50011, United States of America
[4] Ames Laboratory, US Department of Energy, Iowa State University, Ames, IA 50011, United States of America

E-mail: jbelo@fc.up.pt

Received 17 October 2019, revised 11 February 2020
Accepted for publication 25 February 2020
Published 31 March 2020

Abstract

A multi-functional $Gd_5Si_{1.3}Ge_{2.7}$ thin film deposited by pulsed laser ablation in the form of an ensemble of nanoparticles was studied for 18 thermal cycles via electron transport measurements together with structural and magnetic characterization. A general negative thermal dependency of the resistivity (ρ) is observed, which contrasts with the metallic-like behavior observed in bulk $Gd_5Si_xGe_{4-x}$ compounds. This general trend is interrupted by a two-step, positive-slope transition in $\rho(T)$ throughout the [150, 250] K interval, corresponding to two consecutive magnetic transitions: a fully coupled magnetostructural followed by a magnetic order on heating. An avalanche-like behavior is unveiled by the $\partial\rho/\partial T(T)$ curves and is explained based on the severe strains induced cyclically by the magnetostructural transition, leading to a cycling evolution of the transition onset temperature ($\partial T''_h/\partial n \sim 1.6$ K/cycle, n being the number of cycles). Such behavior is equivalent to the action of a pressure of 0.56 kBar being formed and building up at every thermal cycle due to the large volume induced change across the magnetostructural transition. Moreover the thermal hysteresis, detected in both ρ and magnetization versus temperature curves, evolves significantly along the cycles, decreasing as n increases. This picture corroborates the thermal activation energy enhancement—estimated via an exponential fitting of the $\partial\rho/\partial T(T)$ in the avalanche regime. This work demonstrates the importance of using a short-range order technique, to probe both magnetic and magnetostructural transitions and their evolution with thermal cycles.

Keywords: magnetocaloric effect, magnetic refrigeration, phase transitions, magnetic nanoparticles, martensitic phase transition, transport phenomena, dynamics of phase separation

(Some figures may appear in colour only in the online journal)

1. Introduction

There has been a recent interest towards the micro and nano-scales opportunities for multifunctional materials [1–3]. In particular, for materials with strong magnetostructural coupling, such size-reduction effort can prompt new applications as well as help unveil their complex magnetostructural transitions through different methods and analysis. Since the discovery of the giant magnetocaloric effect (GMCE) at room temperature on $Gd_5Si_2Ge_2$ bulk compound by Pecharsky and Gschneidner Jr [4], the $R_5(Si_xGe_{1-x})_4$ (R = rare-earth) family has been subjected to intensive research [5–7]. The GMCE

results from the strong spin lattice coupling present in these materials, which leads to magnetostructural transitions with large heat release or absorption (when magnetic field is applied or removed, respectively) [8]. Their transition temperature can be adjusted by substituting the rare earth element or by tuning the Si, Ge concentration (x) [9–11]. Despite the remarkable MCE, their large magnetic hysteresis combined with the heavy rare-earths increasing prices constitute an effective limitation on the scale-up processing of these materials. However, their multi-stimuli and highly responsive properties such as, giant magnetoresistance [12], colossal magnetostriction [8, 13] and large barocaloric effect [14] are of high-level scientific interest. In particular, fundamental physical questions remain unknown, including the intriguing martensitic-like magnetostructural transitions these materials undergo, their dynamic behavior and their dependence on microstructural features (critical-size limit, grain boundaries). In fact, such fundamental questions are universal to other strongly magnetovolume coupled materials [15], such as Mn–Fe–P–Si [16], La–Fe–Si [17] and their hydrides [18] and the Heusler alloys [19]—all with potential use in new caloric applications and related technologies [20, 21]. Therefore the importance of having a deeper knowledge on martensitic-like transitions is extensive to the whole multifunctional materials field. In the last 10–20 years a huge and successful effort was made in the static or quasi-static characterization of these materials, however, significantly less attention was given to the materials behavior under large number of cycles (mimicking a real-life device), which are crucially important for technological applications, such as magnetic refrigeration among others [22, 23]. Such studies become even more critical as these materials strong spin-lattice coupling normally implies huge structural changes. In particular, Sousa and coworkers [24], have performed a thorough electrical resistance measurements study under thermal cycling on a $Gd_5Si_{0.4}Ge_{3.6}$ bulk compound, concluding that the martensitic-like transition evolves through a sequence of discontinuous steps or avalanches. In parallel, Pérez-Reche and coworkers detected the acoustic emission across the magnetostructural transition of a $Gd_5Si_2Ge_2$ sample, confirming its burst-like character and evidencing the differences between heating and cooling cycles [25]. Waske and coworkers noticed the transition asymmetry between cooling and heating protocols on a La–Fe–Si sample highlighting the importance of such features on the performance of a magnetocaloric material (MC) in a real-life device [26]. Although a variety of interesting and useful techniques have been applied in these studies, herein we highlight the electrical transport measurements given its short range nature, associated with the electron mean free path (nanometer scale), which allows to access detailed information on the mechanisms ruling these transitions at the micro and nanoscale [27–29]. So far, only the works devoted to bulk compounds were mentioned, however an increasing research task force is being dedicated to study these materials at the micro and nano scales. Recently, FeRh mesostructures (micron-sized stripes) with large surface/volume ratio were studied by Uhlír and co-workers, who unveiled a strong thermal asymmetry and an avalanche-like nature of their magnetostructural transition [30]. In addition to microdevice refrigeration, including solid-state microrefrigerators [20] with thermal switches [21], the micro and nanoscale magnetocaloric materials have a wide range of applications such as magnetic nanofluids [31], flexible energy harvesting devices [32], hyperthermia cancer treatment [33] and negative thermal expansion [34] as thorougly reviewed in the following references [1, 3, 35–37]. In the past few years, our team has been focused on the size-confinement of the $R_5(Si_xGe_{1-x})_4$ compounds [34, 38–41] with a particular focus on the transitions kinetics and their evolution with both thermal cycles [41] and heat treatments [40]. As the micro and nanoscale miniaturization is still at an early stage, there are many open questions to be answered. In this work we aim to contribute to answer the following questions: what are the differences between a magnetostructural and a magnetic transition evolution, are there precursor effects or any major asymmetries or is there microcrack formation. In order to reply these, the $Gd_5Si_xGe_{4-x}$ materials were chosen and in particular the $Gd_5Si_{1.3}Ge_{2.7}$ composition, as it presents a giant (0.8%) and anisotropic volume change, a giant magnetocaloric effect and in the granular thin film form presents two decoupled magnetic transitions [38]. At room temperature, the atomic structure of this nanogranular thin film is composed of a mixture of two concurrent orthorhombic phases: O(I) and O(II), with 35 and 65% fractions, respectively. Below 150 K, only the O(I) phase exists, whereas at the magnetostructural transition temperature ($T_{MS} \sim 190$ K) it converts incompletely (65%) into O(II), while 35% remain in the O(I) phase with ferromagnetic order up to $T_C \sim 250$ K. The O(I) has a smaller unit-cell volume (0.8% smaller) than O(II) and their unit cells can be break down in two rigid slabs that lie in the ac plane and are stacked by interslab Ge3↔Ge3 bonding [or its absence in O(II)] along the b axis, as reported in several previous works [5, 6, 9]. Therefore, to tackle the above questions, electrical transport measurements in a wide temperature range [(100, 300) K] and for several thermal cycles (1–18 cycles) were performed on a polycrystalline 800 nm thick $Gd_5Si_{1.3}Ge_{2.7}$ thin film.

2. Experimental details

A polycrystalline 800 nm thick $Gd_5Si_{1.3}Ge_{2.7}$ thin film was grown on top of a SiO_2 (1 μm)/Si substrate through a femtosecond pulsed laser ablation of a polycrystalline $Gd_5Si_{1.3}Ge_{2.7}$ bulk target. More information regarding the thin film production can be found in reference [38]. The electrical resistivity was measured with the standard four-point potentiometric method using a dc current of 2 mA, stable to 1:10^6. The four electrical contacts were established by gold sputtering four points evenly spaced along a straight line and silver paint to bond them together with copper wires on top of a $\sim 3 \times 6$ mm piece cut from the larger deposited thin film. The voltage was measured with a Keithley 182 nanovoltmeter with a resolution of 10 nV during the measurements. The thin film was glued with a thin layer of GE varnish to a massive copper block support in order to minimize any possible temperature gradient, and its electrical resistance (R) was measured uninterruptedly along 18 thermal cycles (cooling and heating) in the [100–300] K temperature range with a

0.5 K min^{-1} rate. The magnetization as a function of temperature measurements were performed in a commercial (Quantum Design MPMS-5S) Superconducting Quantum Interference Device magnetometer with an applied field of 1000 Oe, on cooling and heating in the [5, 300] K temperature interval with a rate of 1.33 K min^{-1}.

3. Experimental results

3.1. Electrical resistivity $\rho(T)$

The [100, 300] K temperature interval was chosen in particular because this range contains the magnetostructural (1st-order) and the magnetic (2nd-order) transitions [38]. Figure 1 displays the results obtained in the 1st, 4th and 18th thermal cycles. One observes that the six $\rho(T)$ curves (3 cooling/heating pairs) overlap almost completely from 100 to 150 K, and above 275 K, both within and between thermal cycles. Within the transition(s) [150–275] K interval, there is a considerable thermal hysteresis in $\rho(T)$ heating and cooling curves and also sudden $\rho(T)$-discontinuities (burst-like processes that will be detailed below). (i) While heating, the intrinsically hysteretic magnetostructural transition [O(I), FM] $\rightarrow$ [O(II), PM] develops smoothly, starting at $\sim$160 K and reaching a maximum rate of change at $T = T_h' = T_h^{ms} \sim 191$ K for the 1st heating run—such T' value remains unaltered up to the 18th cycle. The temperature range where the magnetostructural transition occurs, [150, 200] K, shows no remarkable ρ-discontinuities and retains the same $\rho(T)$ shape under thermal cycling. In contrast, the interval associated with the magnetic transition [200, 250] K, always starts with a sharp ρ-step, observed at $T'' \sim 210$ K in the first heating run. This value shifts considerably to higher temperatures in successive thermal cycles (e.g. $T'' \sim 244$ K in the 18th heating cycle), and some fine details of the transition evolve as well. (ii) While cooling, the magnetic transition is signalled by a smooth descendant beginning $\sim$13 K below the heating curve and then develops in a dense succession of small ρ-irregularities (see in figure 1) which ends at the onset of the interval associated with the magnetostructural transition. There, it evolves by a smoother decreasing behavior whose maximum rate of change is achieved at $T_c' = T_c^{ms} \sim 177$ K. The absolute magnitude of ρ in our film ($\sim$5400 $\mu\Omega$ cm) is very large compared with the commonly reported values for the $R_5(Si_xGe_{1-x})_4$ compounds, $\rho \sim$ 500–1000 $\mu\Omega$ cm in the [100–300] K range [28, 42–44]. This high residual resistivity (ρ_r) is most likely due to the low conductivity between grains and is insensitive to thermal cycling, contrasting with the bulk counterpart cases [24, 27]. Moreover, its low-T and high-T negative $\partial\rho/\partial T$ thermal dependence also contrasts with the typically positive thermal dependence observed in the bulk counterparts. The origin of this negative slope will be discussed below and is detailed in reference [34]. As shown below, one can approximate the residual resistivity by $\rho_r(T) = a - bT$ in the upper temperature range, above 250 K, where $a = 5978$ $\mu\Omega$ cm, $b = 1.768$ $\mu\Omega$ cm K^{-1}. By subtracting $\rho_r(T)$ linear term from the total resistivity $\rho(T)$ measured in the 18th thermal cycle one obtains $\rho'(T) = \rho(T) - \rho_r(T)$ for heating and cooling, as displayed in figure 2.

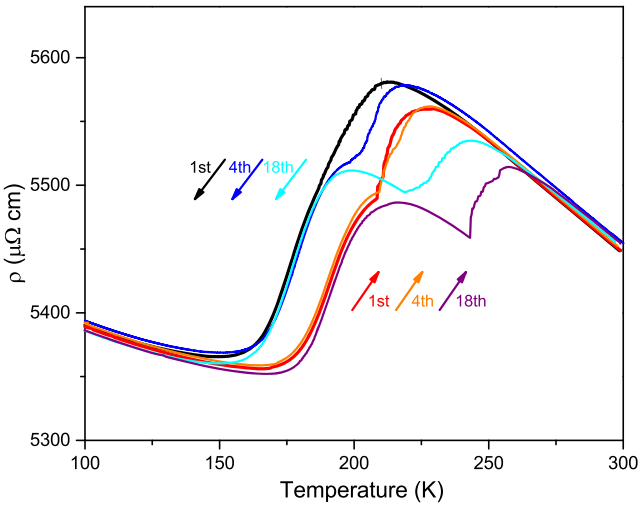

Figure 1. $Gd_5Si_{1.3}Ge_{2.7}$ thin film electrical resistivity as a function of temperature in the 100–300 K temperature range for the 1st, 4th and 18th cooling and heating runs.

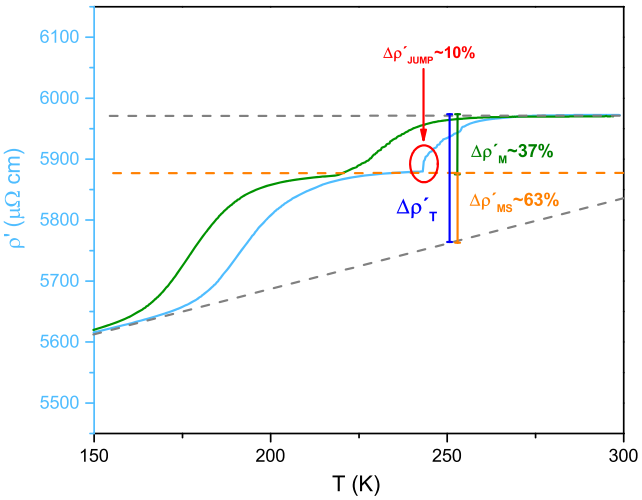

Figure 2. The 18th cycle heating and cooling $\rho'(T)$ curves, obtained by subtracting the high-temperature negative slope of $\rho(T)$. Grey dashed lines are just linear extrapolations of the low and high-temperature regions. The estimated overall $\Delta\rho'_T$ at $T = 250$ K is decomposed in two parts $\Delta\rho'_{MS}$ and $\Delta\rho'_M$. A $\rho_r(T)$ discontinuity is also highlighted in red and is about 10% of the overall variation $\Delta\rho'_T$.

The $\rho(T)$ curves resemble the typical $\rho(T)$ behaviour presented by the $R_5(Si_xGe_{1-x})_4$ compounds and nicely disentangle both transitions and their thermal hysteresis. Furthermore, it also allows to weight the role of each transition on the overall resistivity change as represented in figure 2. One notes that the magnetostructural transition is responsible for $\Delta\rho'_{MS} \sim 63\%$ resistivity variation whereas the magnetic one is responsible for $\Delta\rho'_M \sim 37\%$ of the total resistivity variation across the two transitions, $\Delta\rho'_T$.

3.2. Temperature dependence of $\partial\rho/\partial T$

A better insight into the above features, enabling the disentanglement of finer details of the magnetostructural and magnetic

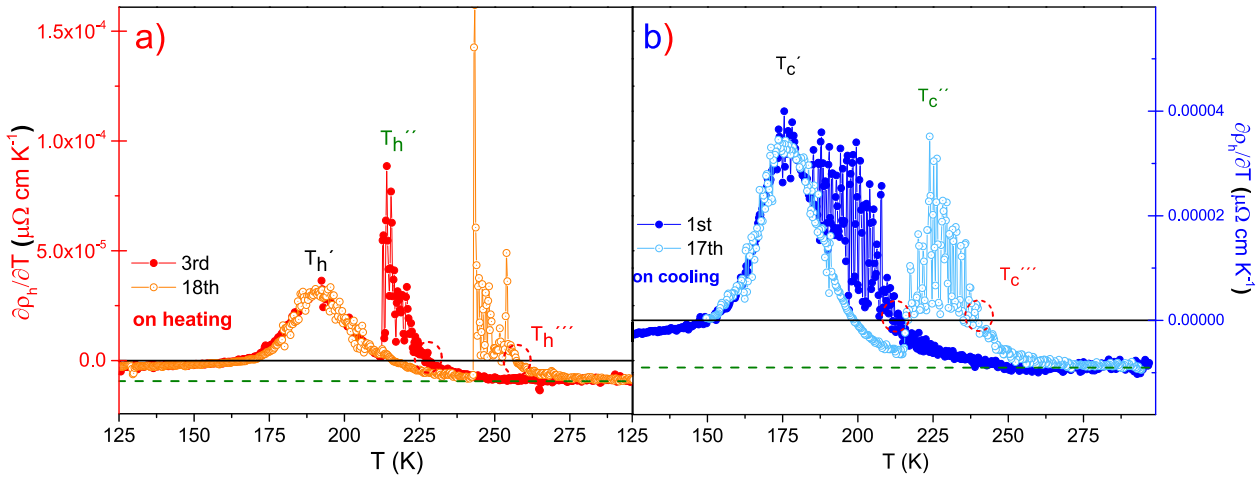

Figure 3. Resistivity temperature derivative, $\partial\rho/\partial T$, in the [125, 300] K interval for the 3rd and 18th heating runs (a) and 1st and 17th cooling runs (b). T' signals the temperatures at which $\partial\rho/\partial T$ is maximum across the magnetostructural transition, i.e. in the [150, 210] K interval. T'' and T''' signal the first spike and the crossover of $\partial\rho/\partial T$ back to negative values, respectively. They represent the onset and the end of the magnetic transition, respectively.

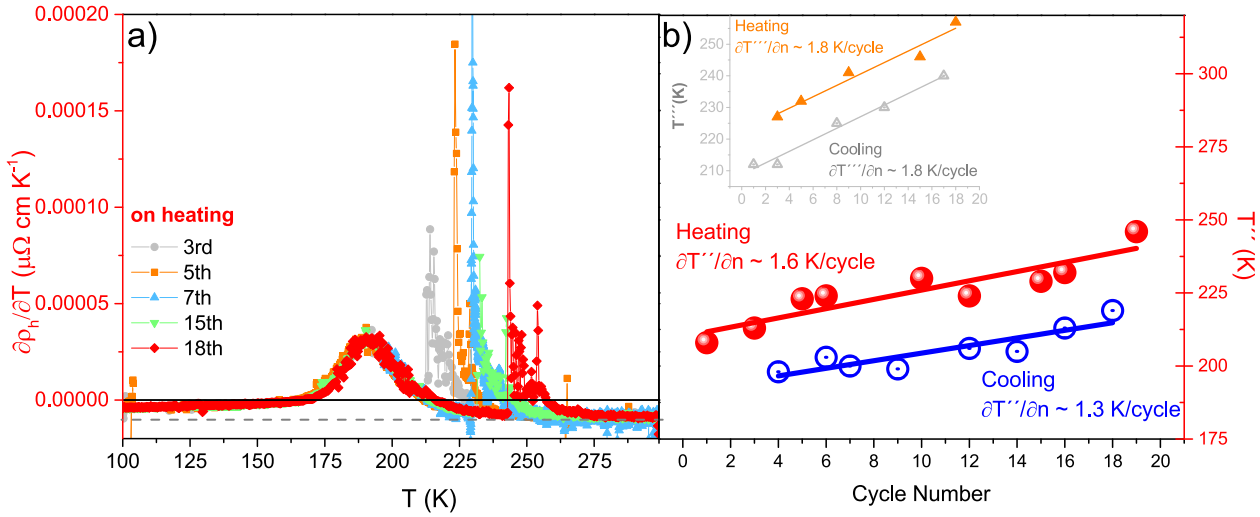

Figure 4. Resistivity temperature derivative, $\partial\rho/\partial T$, in the [100, 300] K interval for the 3rd, 5th, 7th, 15th and 18th heating runs (a). (b) Evolution of T_c'' and T_h'' on the number of cooling and heating runs, respectively. Linear extrapolation estimation gives a 1.3 K/cycle and 1.6 K/cycle, respectively. In figure (b) inset the same linear behavior, with a 1.8 K/cycle slope, is observed for cooling and heating of T''' against the number of runs.

transitions when they partially overlap, can be gained with the analysis of the $\partial\rho/\partial T$ curves.

3.2.1. Heating runs. Figure 3(a) displays $\partial\rho/\partial T$ curves for two heating runs: the 3rd (overlapped transitions) and 18th (separated transitions). The magnetostructural transition produces a smooth and positive Lorentzian-like $\partial\rho/\partial T$ curve, with its peak at $T_h' = T_h^{ms} \sim 191$ K and the same curve shape and magnitude for both runs. Thus, the lattice and the magnetic structures must have the same physical characteristics around T_h^{ms} for all heating runs. In contrast, the magnetic transition starts with a very sharp positive spike in $\partial\rho/\partial T$ at T_h'', equivalent to a ρ-discontinuity. Since it is observable at the macroscopic level this represents an avalanche-type process that affects the electronic duction in the film. Then follows a relaxation-like regime (see figure 6) with a few smaller spikes, which evolve and smoothly fade away. Considering T'' as the abrupt onset of the magnetic transition, under the adopted thermal cycling conditions, one sees that it is considerably shifted to higher temperatures under cycling: $T'' = 213$ K in the 3rd and 246 K in the 18th heating run, as seen in figure 4(b). A more complete set of heating $\partial\rho/\partial T$ curves (3, 5, 7, 15 and 18th) is displayed in figure 4(a) confirming the described characteristics.

3.2.2. Cooling runs. Figure 3(b) displays two $\partial\rho/\partial T$ curves obtained under cooling (1st and 17th runs) with the same time rate as for the heating runs (0.5 K min^{-1}). In general terms, the curves resemble those obtained under heating. In particular, at temperatures sufficiently above T_c' they have the same negative resistivity coefficient, $\partial\rho/\partial T = -8.6 \times 10^{-4}\ \mu\Omega$ cm K^{-1}. With subsequent cooling $\partial\rho/\partial T$ smoothly grows through a

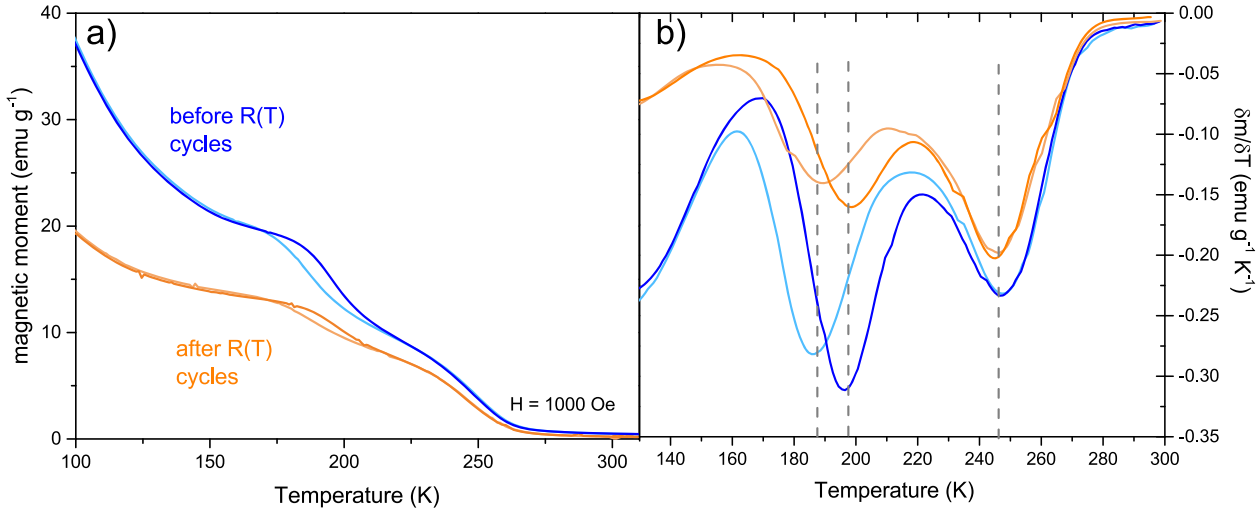

Figure 5. (a) Magnetization as a function of temperature while heating (darker curves) and cooling (lighter curves), before (upper blueish curves) and after (lower and orange curves) the resistivity cycles under an applied magnetic field of $H = 1000$ Oe. (b) Magnetization temperature derivative, $\partial M/\partial T$, as a function of temperature.

relaxation-type regime, as under heating, now described in the opposite sense. As the sample enters the central part of its magnetic transition, a succession of wiggly spikes of similar magnitude develop on top of an average Lorentzian-like $\partial\rho/\partial T$ bump (figure 3(b)). In the 1st run, despite the spiking blur effect overlapping with the forthcoming magnetostructural transition, a rough estimation of its onset is possible: $T_c'' \sim 190$ K. For the 18th run (well separated transitions) one has $T_c'' \sim 219$ K and a well developed Lorentzian-type $\partial\rho/\partial T$ anomaly associated to the magnetostructural transition, with $T_c' \sim 175$ K in all cooling runs. Figure 4(b) shows the linear rise of T'' on heating and cooling versus the corresponding cycle number (n). Regarding T', it keeps the same value for each type of run : $T_c' \sim 175$ K under cooling and $\sim$191 K for heating.

3.3. Magnetization temperature dependence before and after cycling

The thin film magnetization temperature dependence was measured before and after the resistivity cycles, while heating and cooling under a magnetic field $H = 1000$ Oe. As can be seen in figure 5, before and after resistivity cycling curves follow the same path down to around 275 K, where they split, with the magnetization after cycles (m_{af}) lying below the curve before cycles (m_{be}). Their difference increases slightly across the magnetic transition, however the major changes are observed along the magnetostructural transition: (i) $m_{af}(T)$ departs further from the $m_{be}(T)$ and (ii) there is a clear decrease of the thermal hysteresis presented by the both pairs of heating and cooling curves. As is clear from the temperature derivatives curves, $\partial m/\partial T(T)$ no significant change is observed in the transitions (magnetostructural and magnetic) temperatures [defined as the temperatures for which $\partial m/\partial T(T)$ reaches a local minima]. The magnetic transition is only slightly affected by resistivity cycles as can be confirmed by comparison with the two pairs of $\partial m/\partial T(T)$s curves presented in figure 5(b), becoming slightly narrower and less intense. A more drastic change is observed in the shape and intensity of the $\partial m/\partial T(T)$ across the magnetostructural with a large maxima decrease. In fact, after cycling, the maximum of the magnetization temperature derivative occurs at the high-temperature magnetic transition, in clear-cut contrast with the measurements before cycling. Such change can be assigned to the severe strain and consequent induced stress on neighboring particles/crystallites (as will be detailed below) which can be enough to suppress the structural transition on the neighboring particles/crystallites, leading to an arrest of the phase transition and to a phase mixture region in the [200, 250] K temperature interval, similarly to what was observed in other first-order phase transition families [45, 46]. In particular such an arrest phenomena is known to be enhanced in size-confined samples [45, 47, 48]. Another observable feature is the overall magnetization decrease after thermal cycling, which had already been observed in a previous study [41]. Such feature has been assigned to a cycle induced structural disorder mechanism, which corroborates the decrease of long-range crystal order after cycles. The structural disorder leads to an overall magnetization loss at the magnetically ordered states and a consequent increase of the paramagnetic component [41].

3.4. Negative thermal expansion

In order to better understand the overall negative thermal dependence of the $\rho(T)$ curve it is important to correlate it with the unit cell behavior. Hence, the thin film atomic structure temperature dependence was studied by synchroton x-ray diffraction as detailed in a previous work [34]. The diffractograms were obtained as a function of temperature in 5 K step in the [100, 340] K interval. The unit cell parameters were estimated through Rietveld refinements of the mentioned diffractograms, resulting in an unusual thermal dependence. As can be observed in figure 6(b), a negative thermal expansion was observed in two temperature regions—below and above the structural and magnetic transitions, which are here identified as

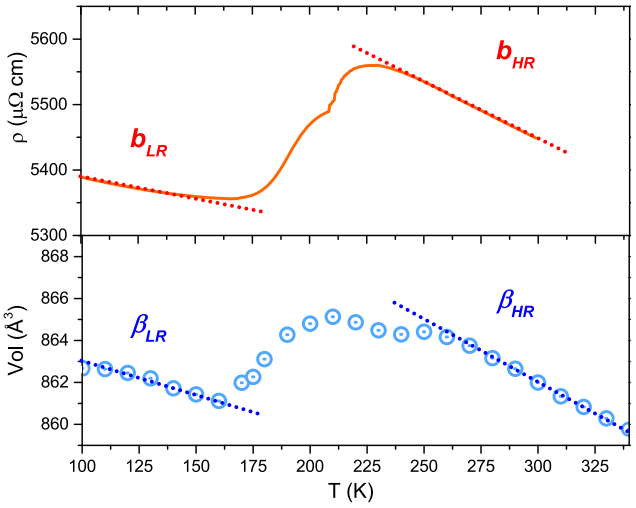

Figure 6. (a) Electrical resistivity as a function of temperature while warming during the 1st cycle. (b) Unit cell volume versus temperature, estimated by Rietveld refinements of several diffractograms measured as a function of temperature.

LR and HR states. Such behavior has been assigned to a size-induced effect that softens the atomic lattice and consequently is expected to change drastically the phonon spectra in comparison with the bulk counterpart. As shown in Figures 6(a) and (b) the resistivity and the unit cell volume evolve generally in a very similar way with temperature: a negative thermal dependence before 150 K, a two-step positive dependence in the [175, 250] K range and again a negative (with larger negative slope) thermal dependence in the [250, 300] K interval. In fact, the ratios of the two slopes (at HR and LR) of the two quantities (ρ and V) result in a very similar value: $(\partial\rho/\partial T_{\mathrm{HR}})/(\partial\rho/\partial T_{\mathrm{LR}}) = b_{\mathrm{HR}}/b_{\mathrm{LR}} \sim 2.25$ and the volume $V(T)$ slopes ratio, $(\partial V/\partial T_{\mathrm{HR}})/(\partial V/\partial T_{\mathrm{LR}}) = \beta_{\mathrm{HR}}/\beta_{\mathrm{LR}} \sim 2.16$. This correlation highlights the sensitivity of the electrical resistivity measurements to crystallographic changes.

4. Analysis and discussion

As a preliminary analysis, an overall comparison between these results and the ones obtained for bulk compounds should be performed. To our knowledge, there are no reports on transport measurements of a bulk $Gd_5Si_{1.3}Ge_{2.7}$ compound, however a comparison can be made with Ge-rich $Gd_5Si_xGe_{1-x}$ compounds. In the $Gd_5Si_{0.4}Ge_{3.6}$ bulk compound [49], an overall high resistivity behavior was found for $T > 50$ K—with a high resistivity (HR) state at higher temperatures and a low resistivity (LR) state at low temperatures. In fact, as reviewed by Mudryk and coworkers [5], such resistivity evolution across a first-order transition is similar in all studied $R_5Si_xGe_{1-x}$ compounds. Moreover, the thermal hysteresis across the first order transitions is commonly observed in bulk electrical resistivity studies, which is caused by the large magnetovolume coupling present in these materials. Despite these common features there is a striking difference to the bulk $\rho(T)$ curves: the negative $\rho(T)$ slope here shown both at the LR and HR states. In the parent compounds the overall electrical resistance exhibits a positive temperature dependency, typical of a metallic behavior.

As shown above, this change in the resistivity thermal dependence (from positive in bulk to negative values at the nanoscale) is a direct consequence of the change in the behavior of the volume thermal expansion. At the nanoscale, the volume thermal behavior assumes an unique negative thermal expansion behavior that contrasts with the conventional positive thermal expansion observed in the bulk counterparts [34]. The $\rho(T)$ and $V(T)$ correlation results from the linear dependence of the phonon contribution to the total resistivity of a metal/alloy on the thermal expansion coefficient [50]. Therefore, the size-induced negative $\rho(T)$ thermal dependence is a direct consequence of the nanoparticles negative thermal expansion.

A closer look at $\rho(T)$ in the LR state evidences that there is a small quadratic contribution, as can be confirmed by the slightly positive linear temperature dependency of $\partial\rho/\partial T(T)$ in this temperature range (figure 3), where $\partial\rho/\partial T = A + BT$. Consequently $\rho(T) = AT + BT^2 + C$. Such a quadratic temperature dependency can be associated with the electron scattering on spin waves (electron–magnon scattering), as was also found on their bulk counterpart [42]. In fact, this hypothesis is reinforced by the constant and temperature-independent $\partial\rho/\partial T$ value observed in the HR state, $\sim -8.6 \times 10^{-4}$ $\mu\Omega$ cm K^{-1}, where no long-range magnetic correlations and consequently no electron–magnon scattering can occur and the typical electron–phonon interaction dominates.

The general evolution from a high resistivity (HR) state at higher temperatures towards a low resistivity (LR) state at low temperatures can be attributed to several mechanisms and here just two of them will be highlighted: (i) the decrease of conduction electrons with the increase of unit cell volume across the magnetostructural transition and (ii) the increase in the electron–phonon scattering above the transition temperature. The former one was firstly explained by Choe and coworkers when they showed, using the Zintl–Klemn formalism, that the isolated Si, Ge atoms and their dimers (Si)Ge–Ge(Si) have different formal charges associated, namely -4×2 and -6e, respectively, i.e. dimmers need less electrons then two unbounded Si, Ge atoms (two electrons less) [52]. Hence, since the LR structure [O(I)] has two dimers formed and the HR structure [O(II)] has none, the corresponding charge balanced formula for the O(I) is $[(Gd^{3+})_5(T_2^{6-})_2(3e^-)]$ whereas for the O(II) is $[(Gd^{3+})_5(T^{4-})_4(-1e^-)]$, resulting in 3 electrons available for the conduction band against one vacancy. In a unit cell, the number of free electrons increases linearly with the number of (Si)Ge–Ge(Si) dimers. Its effect on the resistance behavior had already been pointed out by Sousa and coworkers and Hall measurements consistent with this scenario were performed by Stankiewicz and coworkers [53]. The later effect (ii), proposed by Levin and coworkers, simply argues that, since the higher temperature structures are more loosely bonded and hence more disordered, it means that their electron–phonon scattering will be higher [42]. In comparison with the bulk behavior, the overall resistivity change from the LR to the HR state, $\Delta\rho_T \sim 4\%$ is lower than the

∼20 and 66% observed in the $Gd_5Si_{1.7}Ge_{2.3}$ [54] and $Gd_5Si_{0.4}Ge_{3.6}$ bulk compounds [49]. This smoothing is also noticeable in the temperature window width where the transition occurs (hysteresis area), as it is much larger (∼100 K) than the bulk counterparts (typically ∼40 K). Such broadening and smoothing can be attributed to a phase-separated state resultant of strain disorder—a distribution of volumes implies a distribution of nanoparticles intrinsic strain as explained previously [38] and modeled by Amaral and Amaral [55].

As previously mentioned the two-step nature of the resistivity evolution can be explained by attributing each step to a specific magnetic transition: low temperature step to the magnetostructural transition and high temperature one to the magnetic transition of the arrested O(I) phase. Such correspondence can be made because: (1) the steps and magnetic transitions are coincidental, i.e. occur at the same temperature and (2) as detailed in figure 2, $\Delta\rho'_{MS}$ and $\Delta\rho'_{M}$ are accountable for 63% and 37% of the overall resistivity change, $\Delta\rho'_{T}$, corroborating nicely with the 66% and 33% phase fractions undergoing the magnetostructural and magnetic transition, respectively, estimated by the synchrotron x-ray diffraction data [38].

Concerning the observed $\partial\rho/\partial T$ bursts and the literature on $Gd_5(Si, Ge)_4$ compounds, it is important to remark that their presence had already been reported in electrical resistance, calorimetric and magnetization measurements of Ge-rich $Gd_5(Si_xGe_{1-x})_4$ and $Gd_5(Si_2Ge_2)$ bulk compounds [24, 56, 57], where they were pointed out as fingerprints of an avalanche mode transition. As illustrated by Sousa and coworkers [24], this means that the system evolves through a series of discontinuous steps or avalanches of the order parameter with an associated energy loss and consequent thermal hysteresis, as observed here. Furthermore, it is important to remark the asymmetry between the smoother and the more abrupt avalanche natures during cooling and heating runs, respectively. Such asymmetry is well known in martensitic transformations, where the avalanches are more intense in the reverse direction (heating) than in the forward (cooling) direction [58, 59]. In the Gd_5Si_2, Ge_2 and $La(FeSi)_{13}$ bulk materials [25, 26] the observed asymmetry was inverse, i.e. higher avalanches for cooling, which is caused by the inverted symmetry relations between the high [O(II)] and low temperature [O(I)] atomic structural phases. Although in this case, the avalanche-like behavior appears to be associated with the magnetic order transition, it is important to remark the strong influence of the magnetostructural transition. Severe strains are created due to the large volume changes across the magnetostructural transition both inside each nanoparticle and in between neighboring nanoparticles. We hypothesize that these magnetostructural induced strains are inhibiting the the magnetic transition of the O(I) arrested phase. Eventually, the magnetic transition is carried away abruptly when sufficient thermal energy is provided in avalanche-like steps possibly associated with different sets of similar-size nanoparticles. In order to deepen the understanding of this earthquake-like behavior, the $\partial\rho/\partial T(T)$ data was subtracted to an exponential baseline and was plotted against a relative temperature, $t = T - T''$ as depicted in figure 7. The subtracted $\partial\rho/\partial T$ curve

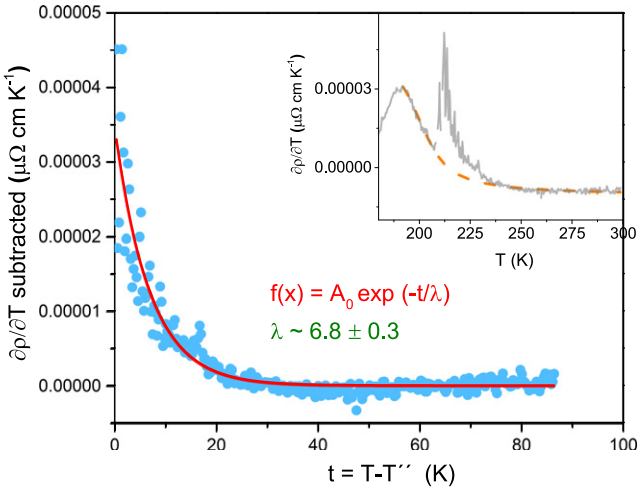

Figure 7. $\partial\rho/\partial T(T)$ for first cycle on heating subtracted by the exponential baseline depicted at the inset as a function of relative temperature $t = T - T''$. The red line represents an exponential law fitting to the subtracted $\partial R/\partial T(T)$ data. In the inset, the associated first cycle $\rho(T)$ data is plotted against absolute temperature.

was fitted with an exponential law, $\partial\rho/\partial T \sim A_0 \exp(-t/\lambda)$, where A_0 is the initial amplitude at T'' and λ represents the relative temperature at which the $\partial\rho/\partial T$ drops down to around one third of its initial value, A_0, i.e. $\partial\rho/\partial T(T'' + \lambda) \sim 0.367A_0$. It was found that both A_0 and λ vary slowly with the thermal cycles, with $\lambda \sim 6.8$ K for the 1st cycle and ∼8.84 K for the 18th cycle. The λ value gives an estimation of the energy involved in these discontinuous local transitions.

To trace the evolution of these avalanches with thermal cycles, the characteristic temperatures that signal the beginning (T'') and end (T''') of this burst-like regime were plotted in figure 4(b). A linear dependency was found for both temperatures, with T''' evolving slightly faster than T'' with the thermal cycles. Moreover T' evolves similarly on heating and on cooling, whereas T'' evolves faster on heating in comparison with cooling experiments. Taking into account the drastic volume changes ($\Delta V/V \sim 1\%$) these nanoparticles undergo across this transition it is possible to conjecture that such transition temperatures evolution is due to the build up of internal stresses associated with each compression–expansion cycle, that eventually completely suppresses the magnetostructural transition as seen previously [41]. According to Morellon and coworkers, an increase in the transition temperature of $\partial T_C/\partial P \sim 3$ K kBar^{-1} is expected for the bulk $Gd_5Si_{0.4}Ge_{3.6}$ (which also undergoes ann O(II)–O(I) structural transition) [60]. The linear and monotonic increase of T''_h (1.6 K/cycle) can be associated with an equivalent pressure of 0.56 kBar occurring every cycle. This picture is further corroborated by the fact that above 200 K, the system is clearly at a phase-separated state and such states are usually very sensitive to stress and other stimuli. Levin and coworkers [27] discarded this explanation as they argue that such a high pressure combined with the brittle nature of these bulk materials would probably destroy the sample. However in this case, the nanoparticles stacking form a lower density material, ensuring more liberty for each nanoparticle to expand and

contract without the formation of any major crack. In fact the absence of crack formation is supported by the constant value of the residual resistance, in contrast to what happens for all $Gd_5Si_xGe_{4-x}$ bulk materials [5, 24, 27]. This picture of the evolution of mechanical stresses, due to adjacent grains undergoing transitions at slightly different temperatures, has been termed as a stress-coupling mechanism and was at the basis of a simulation model used to understand the phase transitions of strongly magnetovolume bulk and loose powders [62]. In a generalized view, this picture suggests that there is a size-induced enhancement of the magnetovolume coupling of the high-temperature transition, associated with an enrichment of the interplay between the two magnetic transitions.

Another interesting feature is the $\sim 25\%$ reduction of the thermal hysteresis area across these transitions. As explained in previous report, the large volume reduction/increase across the structural transition on cooling/heating leads to a gradual arrest of the low-volume phase that hinders the structural transition and eventually suppresses it (after one thousand cycles) [41]. Such effect was also verified in other $Gd_5Si_xGe_{4-x}$ compounds [24, 62] and also in other compounds families presenting a first-order transition, namely the NiMnGa [63] and manganites [64]. In all the cited examples it was always the low-volume phase that became arrested. Sousa and co-workers [24] explained that the complex free energy landscape exhibited by $Gd_5(Si, Ge)_4$ compounds at temperatures near transition are at the origin of mesoscale phase separation. Then the path followed by the system along the transition will be greatly influenced by disorder, which in this case might be represented by inter and intraparticle boundaries, arrested O(I) phase, amorphization, among others. Hence, each time the system crosses the transition it will change this disorder which in turn will change the system percolation path across the transition and the avalanche formation and propagation. Such picture corroborates with the obtained λ increase with the thermal cycles, as the system in order to avoid large energy barriers prefers to evolve in smaller steps that summed up take longer (or demand higher energies) to go trough, but become much more reproducible, as reported by Pérez-Reche [25].

5. Conclusions

In this work, a high resolution transport measurement study was performed on a $Gd_5Si_{1.3}Ge_{2.7}$ thin film deposited by pulsed laser ablation in the form of an ensemble of nanoparticles. This study was extended for 18 thermal cycles allowing to deepen the understanding of the system evolution. A general negative thermal dependency was observed, contrasting with the metallic-like behaviour of bulk $Gd_5Si_xGe_{4-x}$ compounds, which is attributed to a size reduction effect on the thermal expansion behavior (that is positive at the bulk scale, but becomes negative at the nanoscale). This general trend is interrupted by a two-step positive, metallic-like thermal dependency that is caused by two consecutive transitions: a magnetostructural at lower temperatures and a magnetic order at higher temperatures. A strong correspondence between the phase fractions undergoing each transition and the resistivity change across each step can be made. A general picture for the avalanche-like behavior observed in the high temperature step was proposed based on the severe strain induced by the magnetostructural transition. This picture is compatible with the cycle evolution of the temperatures at which the avalanche-like regime begins and ends assuming an internal stress formation that builds up at every thermal cycle due to the large volume induced change across the magnetostructural transition. The magnetic and electrical resistivity thermal hysteresis reduction with thermal cycles was explained via the evolution in smaller steps that require higher energies to go trough, but become much more reproducible. Furthermore, the invariance of the residual resistivity values under cycling, contrasting with the bulk counterparts behavior, is a clear indication of the absence of major cracks in the overall thin film, which might be result of the higher freedom degree in this low-density material. Hence, this work demonstrates the importance of using a short-range order probe, such as the electron mean free path, to sense mesoscopic physical mechanisms. These short-range order techniques will have an enhanced relevance on the inspection of micro and nanostructures as pointed by Miller and co-authors [1] and soundly exemplified by Uhlír and co-workers recent report [30].

Acknowledgments

Work partially supported by the projects POCI/CTM/61284/2004, PTDC/CTM-NAN/115125/2009, FEDER/POCTI No. 155/94 from FundaÇão para a Ciência ex Tecnologia (FCT), Portugal. J H Belo thanks FCT for the Grant SFRH/BD/88440/2012, the project PTDC/FIS-MAC/31302/2017 and his contract DL57/2016 reference SFRH-BPD-87430/2012. A M P thanks FCT for the Grant No. SFRH/BPD/63150/2009. This research was supported by UT Battelle, LLC, under contract No. DE-AC05-00OR22725 for the US Department of Energy, Office of Science.

ORCID iDs

J H Belo https://orcid.org/0000-0003-0010-1568

References

[1] Miller C W, Belyea D D and Kirby B J 2014 Magnetocaloric effect in nanoscale thin films and heterostructures *J. Vac. Sci. Technol.* A **32** 040802
[2] Dunand D C and Mullner P 2011 Size effects on magnetic actuation in Ni-Mn-Ga shape-memory alloys *Adv. Mater.* **23** 216–32
[3] Belo J H, Pires A L, Araujo J P and Pereira A M 2019 Magnetocaloric materials: from micro-to nanoscale *J. Mater. Res.* **34** 134
[4] Pecharsky V K and Gschneidner K A Jr 1997 Giant magnetocaloric effect in $Gd_5Si_2Ge_2$ *Phys. Rev. Lett.* **78** 4494–97
[5] Mudryk Y, Pecharsky V K and Gschneidner K A Jr 2014 *Handbook on the Physics and Chemistry of Rare Earths Includind Actinides* vol 44 (Amsterdam: North-Holland)

[6] Belo J H, Pereira A M, Magen C, Morellon L, Ibarra M R, Algarabel P A and Araujo J P 2013 Critical magnetic behavior of magnetocaloric materials with the Gd_5Si_4-type structure *J. Appl. Phys.* **113** 133909

[7] Marcano N, Algarabel P A, Fernández Barquín L, Araujo J P, Pereira A M, Belo J H, Magén C, Morellón L and Ibarra M R 2019 Cluster-glass dynamics of the Griffiths phase in $Tb_{5-x}La_xSi_2Ge_2$ *Phys. Rev.* B **99** 054419

[8] Morellon L, Algarabel P A, Ibarra M R, Blasco J, García-Landa B, Arnold Z and Albertini F 1998 Magnetic-field-induced structural phase transition in $Gd_5Si_{1.8}Ge_{2.2}$ *Phys. Rev.* B **58** 721–4

[9] Pecharsky V K and Gschneidner K A Jr 2001 $Gd_5(Si_xGe_{1-x})_4$: an extremum material *Adv. Mater.* **13** 683–6

[10] Belo J H *et al* 2012 Tailoring the magnetism of $Tb_5Si_2Ge_2$ compounds by La substitution *Phys. Rev.* B **86** 14403–12

[11] Andrade V M, Belo J H, Reis M S, Costa R M, Pereira A M and Araujo J P 2018 Lanthanum dilution effects on the giant magnetocaloric $Gd_5Si_{1.8}Ge_{2.2}$ compound *Phys. Status Solidi* B **255** 1800101

[12] Morellon L, Stankiewicz J, Garcia-Landa B, Algarabel P A and Ibarra M R 1998 Giant magnetoresistance near the magnetostructural transition in $Gd_5Si_{1.8}Ge_{2.2}$ *Appl. Phys. Lett.* **73** 3462–4

[13] Hadimani R L, Bartlett P A, Melikhov Y, Snyder J E and Jiles D C 2011 Field and temperature induced colossal strain in $Gd_5(Si_xGe_{1-x})_4$ *J. Magn. Magn. Mater.* **323** 532–4

[14] Yuce S, Barrio M, Emre B, Stern-Taulats E, Planes A, Tamarit J-L, Mudryk Y, Gschneidner K A, Pecharsky V K and Manosa L 2012 Barocaloric effect in the magnetocaloric prototype $Gd_5Si_2Ge_2$ *Appl. Phys. Lett.* **101** 071906

[15] Amin D, Belo J H, Amaral V S and Amaral J S 2019 On the optimization of magneto-volume coupling for practical applied field magnetic refrigeration *Phys. Status Solidi* B **256** 1800419

[16] Tegus O, Bruck E, Buschow K H J and de Boer F R 2002 Transition-metal-based magnetic refrigerants for room-temperature applications *Nature* **415** 150–2

[17] Fujieda S, Fujita A and Fukamichi K 2002 Large magnetocaloric effect in $La(Fe_xSi_{1-x})_{(13)}$ itinerant-electron metamagnetic compounds *Appl. Phys. Lett.* **81** 1276–8

[18] Lyubina J, Nenkov K, Schultz L and Gutfleisch O 2008 Multiple metamagnetic transitions in the magnetic refrigerant $La(Fe,Si)_{13}H_x$ *Phys. Rev. Lett.* **101** 177203

[19] Krenke T, Duman E, Acet M, Wassermann E F, Moya X, Mañosa L and Planes A 2005 Inverse magnetocaloric effect in ferromagnetic Ni-Mn-Sn alloys *Nat. Mater.* **4** 450–4

[20] Silva D J, Bordalo B D, Pereira A M, Ventura J and Araújo J P 2012 Solid state magnetic refrigerator *Appl. Energy* **93** 570–4

[21] Puga J B, Bordalo B D, Silva D J, Dias M M, Belo J H, Araújo J P, Oliveira J C R E, Pereira A M and Ventura J 2017 Novel thermal switch based on magnetic nanofluids with remote activation *Nano Energy* **31** 278–85

[22] Lyubina J, Schafer R, Martin N, Schultz L and Gutfleisch O 2010 Novel design of $La(Fe,Si)_{13}$ alloys towards high magnetic refrigeration performance *Adv. Mater.* **22** 3735–9

[23] Wang Y *et al* 2018 Outstanding comprehensive performance of $La(Fe, Si)_{13}H_y$/In composite with durable service life for magnetic refrigeration *Adv. Electron. Mater.* **4** 1700636

[24] Sousa J B, Pereira A M, Correia F C, Teixeira J M, Araujo J P, Pinto R P, Braga M E, Morellon L, Algarabel P A, Magen C and Ibarra M R 2005 Multi-step and anomalous reproducible behaviour of the electrical resistivity near the first-order magnetostructural transition of $Gd_5(Si_{0.1}Ge_{0.9})_4$ *J. Phys.: Condens. Matter* **17** 2461–76

[25] Pérez-Reche F-J, Casanova F, Vives E, Mañosa L, Planes A, Marcos J, Batlle X and Labarta A 2006 Acoustic emission across the magnetostructural transition of the giant magnetocaloric $Gd_5Si_2Ge_2$ *Phys. Rev.* B **73** 014110

[26] Waske A, Giebeler L, Weise B, Funk A, Hinterstein M, Herklotz M, Skokov K, Fahler S, Gutfleisch O and Eckert J 2015 Asymmetric first-order transition and interlocked particle state in magnetocaloric $La(Fe,Si)_{13}$ *Phys. Status Solidi* **9** 136–40

[27] Levin E M, Pecharsky A O, Pecharsky V K and Gschneidner K A Jr 2001 Transformations in the $Gd_5(Si_{1.95}Ge_{2.05})$ alloy induced by the temperature and magnetic-field cycling through the first-order magnetic-martensitic phase transition *Phys. Rev.* B **63** 644261

[28] Pereira A M, Araújo J P, Peixoto J R, Braga M E, Algarabel P A, Magen C, Morellon L, Ibarra M R and Sousa J B 2011 Electron scattering processes in $Ho_5(Si_xGe_{1-x})_4$ compounds: electrical resistivity studies *Phys. Rev.* B **83** 144117

[29] Levin E M, Pecharsky V K, Gschneidner K A and Miller G J 2001 Electrical resistivity, electronic heat capacity, and electronic structure of Gd_5Ge_4 *Phys. Rev.* B **64** 235103

[30] Uhlír V, Arregi J A and Fullerton E E 2016 Colossal magnetic phase transition asymmetry in mesoscale FeRh stripes *Nat. Commun.* **7** 13113

[31] Kitanovski A, Tušek J, Tomc U, Plaznik U, Ožbolt M and Poredoš A 2015 *Magnetocaloric Energy Conversion. Green Energy and Technology* (Cham: Springer)

[32] Cleveland M and Liang H 2012 Magnetocaloric piezoelectric composites for energy harvesting *Smart Mater. Struct.* **21** 047002

[33] Barati M R, Selomulya C, Sandeman K G and Suzuki K 2014 Extraordinary induction heating effect near the first order Curie transition *Appl. Phys. Lett.* **105** 162412

[34] Belo J H *et al* 2019 Giant negative thermal expansion at the nanoscale in the multifunctional material $Gd_5(Si,Ge)_4$ *Phys. Rev.* B **100** 134303

[35] Khovaylo V V, Rodionova V V, Shevyrtalov S N and Novosad V 2014 Magnetocaloric effect in reduced dimensions: thin films, ribbons, and microwires of Heusler alloys and related compounds *Phys. Status Solidi* **251** 2104–13

[36] Doblas D, Moreno-Ramírez L M, Franco V, Conde A, Svalov A V and Kurlyandskaya G V 2016 Nanostructuring as a procedure to control the field dependence of the magnetocaloric effect *Mater. Des.* **114** 214–9

[37] Lyubina J 2011 Recent advances in the microstructure design of materials for near room temperature magnetic cooling (invited) *J. Appl. Phys.* **109** 07A902

[38] Hadimani R L, Silva J H B, Pereira A M, Schlagel D L, Lograsso T A, Ren Y, Jiles D C and Araújo J P 2015 $Gd_5(Si,Ge)_4$ thin film displaying large magnetocaloric and strain effects due to magnetostructural transition *Appl. Phys. Lett.* **5** 32402

[39] Pires A L, Belo J H, Turcaud J, Oliveira G N P, Araújo J P, Berenov A, Cohen L F, Lopes A M L and Pereira A M 2015 Influence of short time milling in $R_5(Si,Ge)_4$, R = Gd and Tb, magnetocaloric materials *Mater. Des.* **85** 32–8

[40] Pires A L *et al* 2015 Annealing influence on the magnetostructural transition in $Gd_5Si_{1.3}Ge_{2.7}$ thin films *Mater. Lett.* **159** 301–4

[41] Pires A L *et al* 2017 Suppression of magnetostructural transition on GdSiGe thin film after thermal cyclings *Thin Solid Films* **621** 247–52

[42] Levin E M 1999 Magnetic-field and temperature dependencies of the electrical resistance near the magnetic and crystallographic first-order phase transition of $Gd_5(Si_2Ge_2)$ *Phys. Rev.* B **60** 7993–7

[43] Hadimani R L and Jiles D C 2010 Resistivity recovery in $Gd_5Si_{2.09}Ge_{1.91}$ by annealing *J. Appl. Phys.* **107** 134–7

[44] Hadimani R L, Melikhov Y, Snyder J E and Jiles D C 2009 Anomalous behavior in electrical transport properties in single-crystal $Gd_5Si_{1.8}Ge_{2.2}$ and polycrystalline $Gd_5Si_{2.09}Ge_{1.91}$ *IEEE Trans. Magn.* **45** 4368–71

[45] Crouigneau G, Porcar L, Courtois P, Lachkar P and Bourgault D 2017 Austenite arrest in polycrystalline Ni-Mn-Co-In films *J. Alloys Compd.* **693** 700–4

[46] Ito W, Ito K, Umetsu R Y, Kainuma R, Koyama K, Watanabe K, Fujita A, Oikawa K, Ishida K and Kanomata T 2008 Kinetic arrest of martensitic transformation in the NiCoMnIn metamagnetic shape memory alloy *Appl. Phys. Lett.* **92** 021908

[47] Keavney D J, Choi Y, Holt M V, Uhlir V, Arena D, Fullerton E E, Ryan P J and Kim J-W 2018 Phase coexistence and kinetic arrest in the magnetostructural transition of the ordered alloy FeRh *Sci. Rep.* **8** 1778

[48] Wu R, Shen F, Hu F, Wang J, Bao L, Zhang L, Liu Y, Zhao Y, Liang F, Zuo W, Sun J and Shen B 2016 Critical dependence of magnetostructural coupling and magnetocaloric effect on particle size in Mn-Fe-Ni-Ge compounds *Sci. Rep.* **6** 20993

[49] Morellon L, Algarabel P A, Magen C and Ibarra M R 2001 Giant magnetoresistance in the Ge-rich magnetocaloric compound, $Gd_5(Si_{0.1}Ge_{0.9})_4$ *J. Magn. Magn. Mater.* **237** 119–23

[50] Palchaev D K, Murlieva Z K, Gadzhimagomedov S H, Iskhakov M E, Rabadanov M K and Abdulagatov I M 2015 Thermal expansion and electrical resistivity studies of nickel and armco iron at high temperatures *Int. J. Thermophys.* **36** 3186–210

[51] Araujo J P *et al* 2005 Transport and magnetic study of the spin reorientation transition in the $Tb_5(Si_{0.5}Ge_{0.5})_4$ magnetocaloric compound *J. Phys.: Condens. Matter* **17** 4941–9

[52] Choe W, Pecharsky V K, Pecharsky A O, Gschneidner K A Jr, Young V G Jr and Miller G J 2000 Making and breaking covalent bonds across the magnetic transition in the giant magnetocaloric material $Gd_5(Si_2Ge_2)$ *Phys. Rev. Lett.* **84** 4617–20

[53] Stankiewicz J, Morellon L, Algarabel P A and Ibarra M R 2000 Hall effect in $Gd_5Si_{1.8}Ge_{2.2}$ *Phys. Rev.* B **61** 12651–3

[54] Raj Kumar D M, Manivel Raja M, Prabahar K, Chandrasekaran V, Poddar A, Ranganathan R and Suresh K G 2011 Effect of Si/Ge ratio on resistivity and thermopower in $Gd_5Si_xGe_{4-x}$ magnetocaloric compounds *J. Magn. Magn. Mater.* **323** 1750–4

[55] Amaral J S and Amaral V S 2014 Disorder effects in giant magnetocaloric materials *Phys. Status Solidi* **211** 971–4

[56] Casanova F, Labarta A, Batlle X, Perez-Reche F J, Vives E, Manosa L and Planes A 2005 Direct observation of the magnetic-field-induced entropy change in $Gd_5(Si_xGe_{1-x})_4$ giant magnetocaloric alloys *Appl. Phys. Lett.* **86** 1–3

[57] Velez S, Hernandez J M, Fernandez A, Macià F, Magen C, Algarabel P A, Tejada J and Chudnovsky E M 2010 Magnetic deflagration in Gd_5Ge_4 *Phys. Rev.* B **81** 064437

[58] Manosa L, Planes A and Cesari E 1989 Acoustic emission amplitude distribution during the martensitic transformation of Cu-Zn-Al alloys *J. Phys. D: Appl. Phys.* **22** 977–82

[59] Baró J, Martín-Olalla J-M, Javier Romero F, Gallardo M C, Salje E K H, Vives E and Planes A 2014 Avalanche correlations in the martensitic transition of a Cu-Zn-Al shape memory alloy: analysis of acoustic emission and calorimetry *J. Phys.: Condens. Matter* **26** 125401

[60] Magen C, Morellon L, Algarabel P A, Ricardo Ibarra M, Arnold Z and Ritter C 2008 Hydrostatic pressure effects in the magnetocaloric compounds $R_5(Si_xGe_{1x})_4$ *Advances in Solid State Physics* vol 42 (Berlin: Springer) pp 241–53

[61] Gottschall T, Benke D, Fries M, Taubel A, Radulov I A, Skokov K P and Gutfleisch O 2017 A matter of size and stress: understanding the first-order transition in materials for solid-state refrigeration *Adv. Funct. Mater.* **27** 1606735

[62] Ouyang Z W, Nojiri H, Yoshii S, Rao G H, Wang Y C, Pecharsky V K and Gschneidner K A Jr 2008 Field-induced magnetostructural transition in Gd_5Ge_4 studied by pulsed magnetic fields *Phys. Rev.* B **77** 184426

[63] Booth R A and Majetich S A 2012 The magnetocaloric effect in thermally cycled polycrystalline Ni-Mn-Ga *J. Appl. Phys.* **111** 134–7

[64] Chatterjee S, Giri S and Majumdar S 2012 Metastability and inverse magnetocaloric effect in doped manganite ($Nd_{0.25}Sm_{0.25}Sr_{0.5}MnO_3$) and ferromagnetic shape memory alloy ($Ni_2Mn_{1.36}Sn_{0.64}$): a comparison *J. Phys.: Condens. Matter* **24** 366001